

Jahn-Teller distortions as a novel source of multiferroicity

Paolo Barone,¹ Kunihiko Yamauchi,² and Silvia Picozzi¹

¹*Consiglio Nazionale delle Ricerche (CNR-SPIN), 67100 L'Aquila, Italy*

²*ISIR-SANKEN, Osaka University, 8-1 Mihogaoka, Ibaraki, Osaka, 567-0047, Japan*

(Dated: April 5, 2024)

The Jahn-Teller effect is a fascinating and ubiquitous phenomenon in modern quantum physics and chemistry. We propose a class of oxides with melilite structure $Ba_2TGe_2O_7$ ($T=V, Ni$) where Jahn-Teller distortions are the main responsible for the appearance of electric polarization. At the heart of the proposed mechanism lies the lack of inversion symmetry displayed by tetrahedrally coordinated transition-metal ions, which allows for the condensation of polar Jahn-Teller distortions, at odds with octahedral coordination typical of conventional ferroelectric oxides with perovskite structure. Since the noncentrosymmetric local environment of transition-metal ions also activates the proposed spin-dependent hybridization mechanism for magnetically-induced electric polarization, proper multiferroic phases with intrinsic magnetoelectric interaction could be realized in this class of low-symmetry materials.

PACS numbers: 77.80.-e, 71.70.Ej, 75.85.+t

I. INTRODUCTION

Jahn-Teller (JT) distortions represent a universal mechanism by which spontaneous symmetry breaking may occur in condensed-matter systems. Colossal magnetoresistance in manganites has been explained invoking an essential role of the Jahn-Teller effect¹, which has been also invoked in several high-temperature oxide and fullerene superconductors^{2,3}. Even though JT distortions are nonpolar in the perovskite ABO_3 structure displayed by many ferroelectric oxides, the ferroelectric transition in these systems has been also explained in terms of a pseudo Jahn-Teller (PJT) instability which can take place whenever the vibronic coupling between the ground and excited states is sufficiently strong⁴. The cooperative PJT effect in ferroelectrics has been known for a long time, nevertheless its possible realization in multiferroic perovskite oxides, showing the simultaneous presence of magnetic and ferroelectric ordering, has been only recently suggested⁵⁻⁸. Interestingly, such mechanism defies the empirical exclusion rule, according to which proper ferroelectricity and magnetism should be chemically incompatible and mutually exclusive⁹.

On the other hand, the quest for sizeable magnetoelectric (ME) effects has been pursued in the last decade mainly among magnetically induced improper ferroelectrics, where the microscopic ME interaction is expected to be intrinsically large. In this respect, a very interesting class of materials has been recently object of intense research activity, suggesting a local origin of ME coupling in low-symmetry crystals through a spin-dependent hybridization mechanism¹⁰⁻¹⁵. Essentially, the lack of inversion symmetry in the point group of the transition-metal ions may drive the appearance of local dipoles via an anisotropic hybridization, modulated by the atomic spin-orbit coupling, between the transition-metal ions and the surrounding oxygens. Materials belonging to the melilite family, with general formula $A_2TB_2O_7$ (A^{+2} alkaline metal, T^{+2} tran-

sition metal, $B^{+2} = Si, Ge$), consisting of B_2O_7 dimers linked by TO_4 tetrahedra, represent an interesting playground, where the local properties of T^{+2} cations with tetrahedral coordination could be explored in details. Among these, several compounds have been already synthesized, i.e. $Ba_2TGe_2O_7$ ($T = Mn, Co, Cu$)^{12,16} and $A_2CoSi_2O_7$ ($A = Sr, Ca$)^{17,18}. Due to the lack of inversion symmetry and to the quasi-two-dimensional character of their magnetic interactions, these materials have been predicted to host peculiar incommensurate magnetic spiral ordering¹⁹ and skyrmion excitations²⁰, multiferroicity and highly non-linear magnetoelectric response^{12,16,18,21}, as well as magnetochiral²² and a giant directional dichroism in resonance with both electrically and magnetically active spin excitations²³. The latter phenomena have been mostly explained in terms of the local ME interaction discussed above; specifically, the multiferroic phase observed in $Ba_2CoGe_2O_7$ has been shown to have an improper origin, the ferroelectric polarization being induced by the magnetic order.

In this respect, a yet unexplored possibility is to consider JT instabilities and possible *proper ferroelectric transition* for T ions showing degenerate electronic states in tetrahedral symmetry. The lack of inversion symmetry of the local tetrahedral environment allows for odd ionic displacements to couple with the degenerate electronic states and, therefore, for symmetry-allowed appearance of local dipole moments. In principle, this could imply proper multiferroicity with intrinsically large ME coupling in the family of melilite oxides. We notice that, despite the possible occurrence of polar JT distortions in crystals without local center of inversion has been known for a long time and experimentally revealed, e.g., in rare-earth oxides (such as $DyVO_4$) or in praseodymium compounds (such as $PrCl_3$)²⁴⁻³¹, so far its relevance in the field of multiferroics has been overlooked. Based on these premises, we first discuss in Section II the Jahn-Teller problem relevant for the tetrahedral units TO_4 appearing in the melilite crystal. On the basis of gen-

eral symmetry considerations, we show that polar JT distortions may locally develop in this structure when JT-active transition-metal ions are considered. Density functional theory (DFT) calculations are then used to propose novel melilite oxides where such polar JT effects can appear, possibly leading to ferroelectric, antiferroelectric or ferrielectric phases, as discussed in Sections III,IV.

II. POLAR JAHN-TELLER EFFECT AT TETRAHEDRAL SITES OF MELILITE STRUCTURE

Due to the quasi-layered structure of the melilite structure, each TO_4 appears to be slightly compressed along the c axis, thus belonging to the tetragonal D_{2d} group. As a consequence of the tetragonal crystal field, transition-metal d states are split into nondegenerate d_{z^2} , $d_{x^2-y^2}$, two-fold d_{yz} , d_{zx} and nondegenerate d_{xy} states. The corresponding Jahn-Teller problem for degenerate d_{yz} , d_{zx} is then expressed as $E \otimes (a_1 + a_2 + b_1 + b_2)$. By introducing the standard symmetrized displacements $Q_0(A_1)$, $Q_a(A_2)$, $Q_1(B_1)$ and $Q_2(B_2)$, describing totally and non-totally symmetric displacements shown in Fig. 1(e)-(h), the vibronic matrix defined on the degenerate electronic states reads⁴:

$$W = \begin{pmatrix} \Delta_1 & \Delta_2 \\ \Delta_2 & -\Delta_1 \end{pmatrix}, \quad (1)$$

where

$$\begin{aligned} \Delta_1 &= F_1 Q_1 + L_2 Q_a Q_2 + G_1 Q_1 Q_0 \\ \Delta_2 &= F_2 Q_2 + G_2 Q_0 Q_2 + L_1 Q_1 Q_a, \end{aligned} \quad (2)$$

including both linear F_1, F_2 and quadratic $G_i \equiv G(A_1 \times B_i), L_i \equiv G(A_2 \times B_i)$ couplings. Notice that the non-totally symmetric Q_1 and Q_2 modes describe a nonpolar and polar displacement, respectively, as highlighted in Figs. 1(g)-(h). Upon inclusion of the elastic term $H_0 = (1/2) \sum_i K_i Q_i^2$, the leading distortions as a function of all vibronic parameters can be obtained by minimizing the corresponding energy $\mathcal{E} = \frac{1}{2} \sum_i K_i Q_i^2 \pm \sqrt{\Delta_1^2 + \Delta_2^2}$. Analytical solutions are found only when the quadratic L_i couplings are neglected; however, all modes Q_i of the full JT problem can be obtained as a function of the stationary electronic states, namely of the mixing angle φ through which the ground state is expressed as $|\psi\rangle = \cos \varphi |yz\rangle + \sin \varphi |zx\rangle$ ³².

When $L_i = 0$, two kinds of energy minima are found, where only one of the non-totally symmetric modes with B_1 and B_2 symmetry is activated, either $Q_1 = 0, Q_2 \neq 0$ or $Q_1 \neq 0, Q_2 = 0$, depending on the ratio between linear vibronic and elastic energies $K_2 F_1^2 \gtrless K_1 F_2^2$ as shown in Fig. 1(a), (c) and later on labeled as case a and b , respectively⁴. In terms of the electronic wavefunctions, the two energy minima correspond to $\varphi_a = \pm\pi/4$ (case a) and $\varphi_b = 0, \pi$ (case b), i.e. to a symmetric mixing of d_{yz}, d_{zx} states or to split levels with d_{yz} or d_{zx} unique

character, respectively. On the other hand, when $L_i \neq 0$ an effective coupling between nonpolar and polar modes appears through a term $(F_1 L_2 + F_2 L_1) Q_a Q_1 Q_2$ in the adiabatic potential energy \mathcal{E} . As a consequence, all distortion modes are found to be nonzero at energy minima, thus implying that a polar displacement is always symmetry-allowed, as shown in Fig. 1(1); at the same time, JT split states display an asymmetric mixing of d_{yz} and d_{zx} . Furthermore, the switching of Q_2 (hence of the local dipole) implies a change of sign of the product $Q_a Q_1$, consistently with the trilinear term coupling the two nonpolar and the polar modes. As a consequence, the energy barrier related to the dipole switching can in principle be much reduced with respect to the case of a single-mode instability [see, e.g., Fig. 1 (d)].

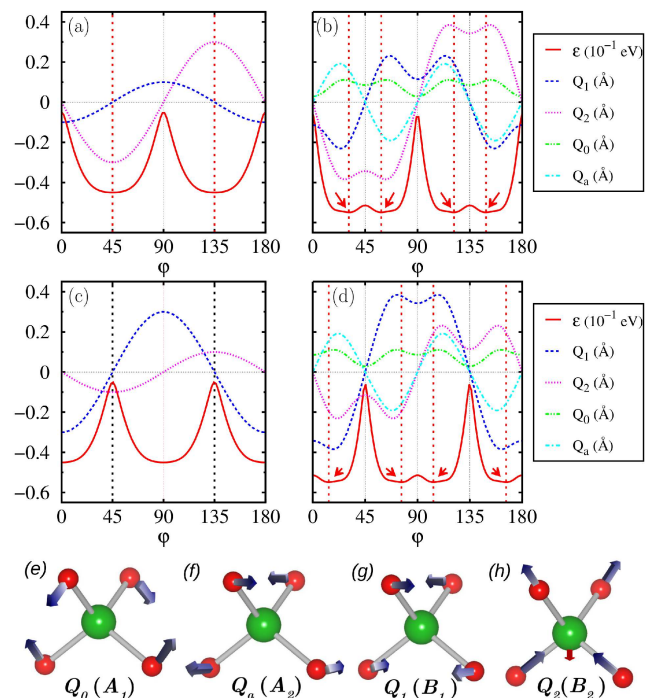


FIG. 1. (a)-(d): Typical evolution of JT modes — shown in panels (e)-(h) — and energy as a function of the electronic angle φ for linear and quadratic couplings. Parameters have been chosen as $K_1 = K_2 = K_a/2 = K_0/2 = 1$ eV/Å², $F_1 = 0.3(0.1)$ eV/Å, $F_2 = 0.1(0.3)$ eV/Å in top (bottom) panels, corresponding to cases a and b discussed in the main text. Quadratic coupling constants are set to zero in left panels (a),(c), while $L_1 = L_2 = 0.9$ eV/Å² and $G_1 = G_2 = 0.5$ eV/Å² in right panels (b), (d). Arrows and vertical lines highlight the energy minima. (e)-(f): Schematic representation of the symmetrized displacements in each tetrahedral unit, corresponding to totally symmetric displacements with symmetry A_1 (e) and A_2 (f), and to non-totally symmetric displacements with symmetry B_1 (g) and B_2 (h).

III. JAHN-TELLER EFFECT IN $\text{Ba}_2\text{NiGe}_2\text{O}_7$

On the basis of the previous general analysis, we consider a hypothetical melilite oxide hosting JT-active T ions, where the polar JT effect previously discussed is expected to appear. We performed DFT calculations resorting to the VASP code³³ within the framework of generalized gradient approximation GGA-PBE, while the electronic correlation has been also taken into account by using the GGA+ U potential³⁴ (with $U=2, 4$ or 6 eV for T ions). Electric polarization has been evaluated in the framework of the Berry-phase approach³⁷. We started from the experimental crystal structure of $\text{Ba}_2\text{CoGe}_2\text{O}_7$ belonging to $P\bar{4}2_1m$ space group³⁵ and fully optimized it by substituting Co with the JT-active ion Ni^{2+} while imposing different magnetic configurations of the transition-metal magnetic moments. We also considered V^{2+} , whose electronic configuration is physically equivalent to Ni^{2+} , but with occupied majority spins only. Indeed, results for both systems show qualitatively the same behavior, therefore we discuss here only the case of $\text{Ba}_2\text{NiGe}_2\text{O}_7$ (BNGO).

In Fig. 2(d), we show the density of states of BNGO decomposed into d orbital states, as obtained when a C-type antiferromagnetic configuration is imposed (similar results are obtained with other higher-energy magnetic configurations). When keeping the same space group $P\bar{4}2_1m$ of the parent compound, BNGO clearly shows a metallic behavior, arising from the twofold degeneracies of (d_{yz}, d_{zx}) orbital states which are half-filled in the minority spin manifold of $\text{Ni}^{2+}(d^8)$, being $e_g^\uparrow t_{2g}^\uparrow t_{2g}^\downarrow t_{2g}^\downarrow$. The degeneracy can then be lifted by a JT structural distortion; indeed, we found that lowering the symmetry to c -centered $Cmm2$ space group leads to the opening of an energy gap in the BNGO compound, being $E_g = 0.3$ (2.3) eV at the bare GGA (GGA+ U , $U=4$ eV) level, with a corresponding total energy gain of 78 (753) meV per formula unit (f.u.). We notice that the main effect of a finite U in the GGA+ U approach is to induce a larger gap and a larger energy gain associated to the structural transition. Both the Ni-O bond lengths and O-Ni-O bond angles are differentiated, as shown in Fig. 3 (b). Two short s (long l) bonds can be identified, linking the Ni ion with upper (lower) lying oxygens in the tetrahedral cage, being $s=1.95$ Å and $l=2.00$ Å ($s=1.97$ Å, $l=1.98$ Å for $U=4$ eV). Furthermore, the $\text{O}^{\text{top}}\text{-Ni-O}^{\text{btm}}$ bond angles β , comprising upper- and lower-lying oxygens, differentiate in $\beta'=106.1^\circ$ (107.6° for $U=4$ eV) and $\beta''=103.0^\circ$ (102.5° for $U=4$ eV), suggesting that the JT-induced distortions do not consist only in a Ni offcentering. Indeed, the ionic displacement from the $P\bar{4}2_1m$ to the $Cmm2$ structure can be decomposed³⁶ into a totally symmetric Γ_1 mode, with total amplitude $Q_{\Gamma_1} = 0.02$ Å, and a distortional (non-totally symmetric) mode, with total amplitude $Q_{\Gamma_3} = 0.13$ Å. The latter displacement mode can be further decomposed in two modes belonging to B_1 and B_2 symmetry representations, shown in Fig. 3(c) and corresponding to those shown in Fig. 1(g),(h),

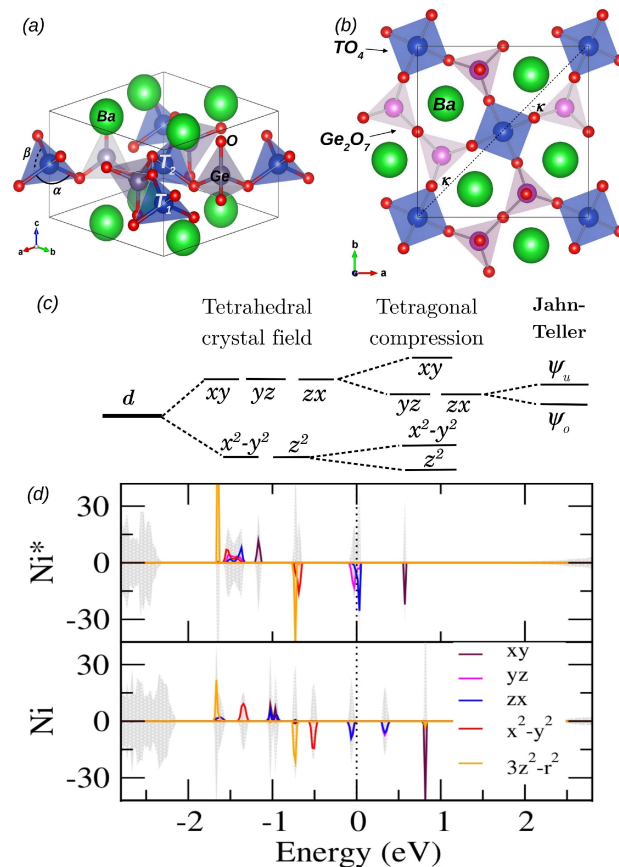


FIG. 2. (a) Melilite crystal structure of $\text{Ba}_2T\text{Ge}_2\text{O}_7$ with $P\bar{4}2_1m$ symmetry, showing layers of Ge_2O_7 dimers linked by TO_4 tetrahedra intercalated by Ba ions. The TO_4 tetrahedra are compressed along the c axis, resulting in different O-T-O angles α, β . (b) Top view of the crystal structure, highlighting two inequivalent TO_4 tetrahedra which are rotated about the c axis of $\pm\kappa$, respectively. (c) Level structure of T^{2+} metal ion in the melilite crystal. In the tetrahedral environment, d orbitals split into lower e_g and higher t_{2g} manifolds; a tetragonal compression further split the e_g, t_{2g} levels, leaving only twofold degenerated d_{yz}, d_{zx} states. If these levels are half-occupied, as in the case of $\text{Ni}(d^8)$ or $\text{V}(d^3)$, a JT distortion can take place, removing the only left degeneracy. (d) Density of states (States/eV) decomposed into d orbital states and calculated within the bare GGA approach. “Ni*” refers to the parent-compound structure, belonging to space group $P\bar{4}2_1m$, while the optimized distorted structure with $Cmm2$ symmetry is labeled by “Ni”.

in perfect agreement with our previous qualitative analysis. These modes display significant ionic displacements of O ions around the Ni cation, being $Q_{B_1} = -0.10$ Å and $Q_{B_2} = 0.05$ Å. Upon structural distortion, the degenerate yz, zx states are split into occupied $0.61|yz\rangle - 0.79|zx\rangle$ and unoccupied $0.79|yz\rangle + 0.61|zx\rangle$ states, implying a mixing angle $\varphi = 37.7^\circ$. From the point of view of structural distortions, the B_1 mode, differentiating both the bond angle and the bond length, appears as the largest

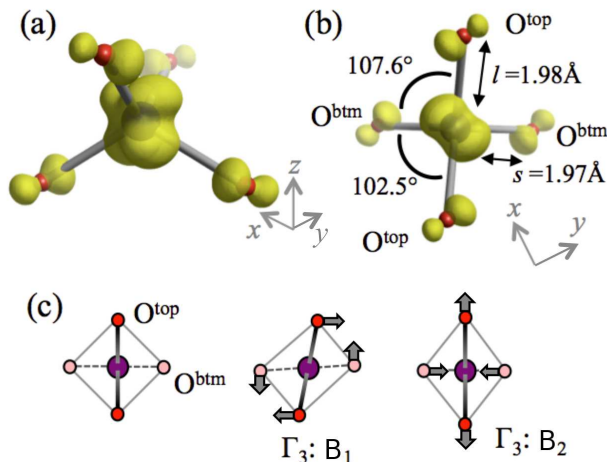


FIG. 3. Charge density plot (obtained within the GGA+ U approach, with $U=4$ eV) corresponding to the highest occupied state of Ni- d state hybridizing with tetrahedral O- p states, (a) in perspective view in a local xyz frame, (b) projected onto the xy plane. (c) Distortion modes of tetrahedral O ions surrounding Ni ion, projected onto the xy plane, as obtained using the ISODISTORT program³⁶.

JT mode; however, the electronic mixing angle appears closer to the value $\varphi_a = \pi/4$ of case a , suggesting that indeed the leading JT distortion arises from mode B_2 , which is the main responsible for the d -orbital state splitting. On the other hand, the simultaneous activation of both B_1 and B_2 modes, alongside the nonzero amplitude of the totally symmetric displacement, points to a non-negligible quadratic couplings L_i , which is further confirmed by the asymmetric mixing of the d_{yz} and d_{zx} orbital states.

IV. MULTIFERROICITY IN JAHN-TELLER MELILITES

If on the one hand the appearance of local dipoles in TO_4 cage can be understood in terms of JT effect, on the other hand the onset of an ordered ferro- (FE) or antiferroelectric (AFE) phase is related to non-local interactions between the different tetrahedral units. Since there are two TO_4 tetrahedra in the parent unit cell, two possible structural configurations can be considered which realize the previously discussed local JT effect ; i) both T ions offcenter downward or upward (FE, $P_c \geq 0$, space group $Cmm2$), ii) T ions offcenter in opposite directions (AFE, $P_c = 0$, space group $P2_12_12_1$). As listed in Tab. I, the AFE structure in both compounds is energetically more stable by 20-30 meV/f.u.. The antiferro character of the cooperative JT interactions can be qualitatively understood in terms of the local coupling between on-site JT distortions. In fact, the sign of the polar distortion Q_2 is determined by the product $Q_a Q_1$, where the first

nonpolar distortional mode is associated with a global rotation of the tetrahedral unit and the second to the antiphase rotation of O^{top} and O^{btm} around the tetrahedral z axis, as shown in Figs 1(f) and (g), respectively. The sign of Q_a is opposite in the two TO_4 units, which are rotated by an angle $\pm\kappa$ in the melilite crystal; on the other hand, Q_1 is expected to display the same sign, in order to minimize the energetic cost associated with distortions of the Ge_2O_7 dimers linking the JT-active units by inducing less asymmetric changes of the O-Ge-O bond angles. The opposite sign of $Q_a Q_1$ thus may explain the observed antiferro configurations of local dipoles associated with the Q_2 local modes. However, one can resort to a different JT ion occupying T sites, such as V^{2+} . Indeed, when combining V and Ni ions, each carrying a different electric dipole, a ferroelectric configuration can be expected, as we show in Tab. I. On the other hand, the substantially local mechanism leading to the formation of electric dipoles suggests that ferroelectric behavior could be in principle attained when doping melilite oxides with JT-active ions; indeed, good-quality crystals of $Ba_2Cu_{1-x}Ni_xGe_2O_7$ have been successfully synthesized up to Ni concentrations of $x = 0.5$, their structural and magnetic characterization being under way^{38,39}.

		ΔE (meV/f.u.)	P_c ($\mu C/cm^2$)
BNGO	PE	775.9	-
	FE	22.9	1.18
	AFE	0	0
BVGO	PE	675.3	-
	FE	30.3	1.90
	AFE	0	0
B(V,N)GO	PE	339.7	-
	strong FE	189.7	-10.85
	weak FE	0	0.70

TABLE I. Relative GGA+ U ($U=4$ eV) total energies and bulk polarization for paraelectric metallic (PE), FE and AFE configurations in BNGO, $Ba_2VGe_2O_7$ (BVGO) and an ordered half-doped $Ba_2V_{0.5}Ni_{0.5}Ge_2O_7$ (B(V,N)GO) hypothetical compound, where the parallel(antiparallel) configuration of inequivalent electric dipoles results in a strong(weak) FE phase.

As for the magnetic properties, we found that both Ni and V oxides display an antiferromagnetic ground state, and therefore they can be considered as proper multiferroic materials. The in-plane exchange constant J_{ab} appears to be the dominant antiferromagnetic interaction, while the out-of-plane exchange J_c changes from ferro- to antiferromagnetic interaction when Ni is replaced by V, leading to C-type and G-type AFM configurations, respectively. In both cases, the estimated exchange anisotropy is rather strong, being $J_c/J_{ab} \lesssim 0.05$, thus displaying the quasi-2D character observed in known parent compounds. On the other hand, the most important contribution to the local spin-dependent hybridization mechanism mediating the reported large ME interaction in melilite oxides has been shown to arise from d_{yz} , d_{zx} orbital states of the T ions¹⁴. Since these states

are partially filled in JT melilites, a significant spin-dependent modulation of charge density at lower- and upper-lying O ions through the asymmetric pd hybridization is expected to further contribute to the local electronic polarization, i.e., to mediate a ME interaction. Due to the partial occupancy of the active d states of T ions, such ME interaction can be in principle of the same order of magnitude of that predicted for Co and Cu compounds, if not larger. Even though the relatively weak exchange interactions are responsible for very low Néel temperatures, signatures of such ME coupling are expected to be visible even in the paramagnetic phase, due to the localized nature of its microscopic origin.

V. CONCLUSIONS

By combining symmetry-based JT analysis and DFT calculations, we put forward a novel mechanism for multiferroicity and theoretically predict the possibility of realizing proper FE and AFE phases in melilite oxides. We have shown that JT instabilities of noncentrosymmetric units can lead to polar distortions and possibly mediate a (anti)ferroelectric transition of proper character which could be signalled by large anomalies in the dielectric susceptibility. The cooperative JT origin of such structural transition is also known to lead to enhanced electrostric-

tive and magnetostrictive responses, that are expected to develop even if the predicted JT distortions display a dynamical, rather than static, character²⁴. Remarkably, the JT polar distortions can be realized in the presence of a magnetic phase, thus circumventing the empirical exclusion rule between magnetism and ferroelectricity usually invoked for perovskite oxides. On the other hand, due to the proper nature of the predicted structural distortions, they are expected to take place at higher temperatures than those typically found for magnetically-induced improper ferroelectrics, at the same time displaying an intrinsic ME interaction of local origin that could be detectable even above the magnetic transition temperature.

ACKNOWLEDGMENTS

P.B. thanks Dr. R. Fittipaldi and Dr. A. Vecchione for useful and fruitful discussions. This work has been supported by CNR-SPIN Seed Project PAQSE002 and MIUR-PRIN Project “Interfacce di ossidi: nuove proprietà emergenti, multifunzionalità e dispositivi per l’elettronica e l’energia” (OXIDE). DFT calculations were performed using the facilities of the Supercomputer Center, Institute for Solid State Physics, University of Tokyo.

-
- ¹ *Colossal Magnetoresistive Manganites*, ed. T. Chatterje (Springer 2004).
- ² *Vibronic interactions: Jahn-Teller effect in Crystal and Molecules*, eds. M.D. Kaplan and G.O. Zimmerman, Nato Science Series II, Vol. 39 (Springer 2000).
- ³ *The Jahn-Teller effect*, eds. H Köppel, D. R. Yarkony and H. Barentzen, Series in Chemical Physics, Vol 97 (Springer 2010).
- ⁴ I. B. Bersuker, *The Jahn-Teller effect*, Cambridge University Press 2006.
- ⁵ J. M. Rondinelli, A. S. Eidelson and N. A. Spaldin, Phys. Rev. B **79**, 205119 (2009).
- ⁶ S. Bhattacharjee, E. Bousquet, and P. Ghosez, Phys. Rev. Lett. **102**, 117602 (2009).
- ⁷ P. Barone, S. Kanungo, S. Picozzi and T. Saha-Dasgupta, Phys. Rev. B **84**, 134101 (2011).
- ⁸ I. B. Bersuker, Phys. Rev. Lett. **108**, 137202 (2012).
- ⁹ N. A. Hill, J. Phys. Chem. B **104**, 6694 (2000).
- ¹⁰ T. Arima, J. Phys. Soc. Jpn. **76**, 073702 (2007).
- ¹¹ C. Jia, S. Onoda, N. Nagaosa, and J. H. Han Phys. Rev. B **76**, 144424 (2007).
- ¹² H. Murakawa, Y. Onose, S. Miyahara, N. Furukawa and Y. Tokura Phys. Rev. Lett. **105**, 137202 (2010).
- ¹³ H. J. Xiang, E. J. Kan, Y. Zhang, M.-H. Whangbo, and X. G. Gong, Phys. Rev. Lett. **107**, 157202 (2011).
- ¹⁴ K. Yamauchi, P. Barone, and S. Picozzi, Phys. Rev. B **84**, 165137 (2011).
- ¹⁵ K. Yamauchi, T. Oguchi and S. Picozzi, J. Phys. Soc. Jpn. **83**, 094712 (2014)
- ¹⁶ H. Murakawa, Y. Onose, S. Miyahara, N. Furukawa, and Y. Tokura, Phys. Rev. B **85**, 174106 (2012).
- ¹⁷ M. Akaki, J. Tozawa, D. Akahoshi, H. Kuwahara, J. Phys.: Conf. Ser. **150**, 042001 (2009).
- ¹⁸ M. Akaki, H. Iwamoto, T. Kihara, M. Tokunaga and H. Kuwahara, Phys. Rev. B **86**, 060413(R) (2012).
- ¹⁹ A. Zheludev, G. Shirane, Y. Sasago, N. Koide, and K. Uchinokura, Phys. Rev. B **54**, 15163 (1996).
- ²⁰ A. N. Bogdanov, U. K. Roßler, M. Wolf, and K.-H. Müller, Phys. Rev. B **66**, 214410 (2002).
- ²¹ H. T. Yi, Y. J. Choi, S. Lee, S.-W. Cheong, Appl. Phys. Lett. **92**, 212904 (2008).
- ²² S. Bordács, I. Kézsmárki, D. Szaller, L. Demkó, N. Kida, H. Murakawa, Y. Onose, R. Shimano, T. Rõöm, U. Nagel, S. Miyahara, N. Furukawa and Y. Tokura *et al.*, Nature Phys. **8**, 734 (2013)
- ²³ I. Kézsmárki, N. Kida, H. Murakawa, S. Bordács, Y. Onose, and Y. Tokura, Phys. Rev. Lett. **106**, 057403 (2011).
- ²⁴ M. D. Kaplan and B. G. Vekhter, *Cooperative Phenomena in Jahn-Teller Crystals*, Plenum Press, New York 1995.
- ²⁵ L. N. Pelikh, A. A. Gurskas, Sov. Phys. Solid State **21**, 1223 (1979).
- ²⁶ B. G. Vekhter, M. D. Kaplan, Sov. Phys. JETP **51**, 892 (1980).
- ²⁷ M. J. M. Leask, A. C. Tropper and M. R. Wells, J. Phys. C: Solid State Phys **14**, 3481 (1981).
- ²⁸ H. Unoki, T. Sakudo, Phys. Rev. Lett. **38**, 137 (1977).
- ²⁹ K. Kishimoto, T. Ishikura, H. Nakamura, Y. Wakabayashi and T. Kimura, Phys. Rev. B **82**, 012103 (2010).

- ³⁰ J. P. Harrison, Jan P. Hessler, D. R. Taylor, *Phys. Rev. B* **14**, 2979 (1976).
- ³¹ D. R. Taylor, J.P. Harrison and D.B. McColl, *Physica* **86-88B**, 1164 (1977).
- ³² U. Öpik, M. H. L. Pryce, *Proc. R. Soc. A* **238**, 425 (1957).
- ³³ G. Kresse and J. Furthmüller, *Phys. Rev. B* **54**, 11169 (1996).
- ³⁴ V. I. Anisimov, F. Aryasetiawan and A. I. Lichtenstein, *J. Phys.: Cond. Mat.* **9**, 767 (1997).
- ³⁵ V. Hutanu, A. Sazonov, H. Murakawa, Y. Tokura, B. Náfrádi, and D. Chernyshov, *Phys. Rev. B.* **84**, 212101 (2011).
- ³⁶ B. J. Campbell, H. T. Stokes, D. E. Tanner and D. M. Hatch, *J. Appl. Cryst.* **39**, 607 (2006).
- ³⁷ R.D.King-Smith and D.Vanderbilt, *Phys. Rev. B* **47**, 1651 (1993); R. Resta, *Rev. Mod. Phys* **66**, 899 (1994).
- ³⁸ R. Fittipaldi, L. Rocco, M. Ciomaga Hatnean, V. Granata, M. R. Lees, G. Balakrishnan and A. Vecchione, *J. Crys. Growth* **404**, 223 (2014).
- ³⁹ R. Fittipaldi, L. Rocco, V. Granata and A. Vecchione, private communication.